ROYAL SOCIETY OF CHEMISTRY

PAPER

Check for updates

A high-performance nanofiltration membrane synthesized by embedding amino acids and ionic liquids in cellulose acetate for heavy metal separation

D. Teja Nayak,[a] Vinoth Kumar Raja, [iD][b] G. Arthanareeswaran, [iD] *[a] Tran Dang Khoa [iD][c] and Wirach Taweepreda[d]

Water reclamation is necessary to meet the potable water demand. Heavy metals such as iron, zinc, lead, and copper, particularly in water, pose significant toxicity risks to humans and other biological life. Over the last few years, the contamination level of these heavy metals in water and soils has increased alarmingly. Correspondingly, membrane systems have emerged as a prominent approach to water reclamation. In this study, cellulose acetate (CA) membranes incorporating amino acids (AAs) and ionic liquids (ILs) were fabricated using phase inversion technique and effectively utilized for metal separation. The characterizations of these membranes using FTIR, SEM, TGA, and DSC revealed the presence of various functional groups, changes in surface morphologies, and improvements in thermal stabilities due to AA−IL. The pure water flux (PWF) was increased to 98 L m^{-2} h^{-1} at 4 bar pressure owing to the enhancement of hydrophilicity. The rejection percentage of heavy metal ions for AA−IL (0.5%) incorporated CA membranes was 94%. The rejection rates for ions of the heavy metals copper, zinc, iron, and lead present in the industrial effluent were studied and found to be 89%, 91%, 84%, and 90%, respectively. The rejection capacity of the AA−IL (0.5) incorporated CA membrane was the highest for all the metals. The AA−IL incorporated CA membranes are efficient and effective for nanofiltration to treat heavy metal ion solutions.

Sustainability spotlight

Amino acid (AAs) and ionic liquids (ILs) were incorporated in cellulose acetate (CA) membranes to treat heavy metal ions from industrial wastewater as an efficient and effective membrane filtration technique. The potential impact of the presented work is significant, and it directly or indirectly supports several Sustainable Development Goals (SDGs): SDG 2, SDG 6, SDG 5, SDG 7, SDG 8, SDG 11, and SDG 14 by enabling efficient water recycling, accessing clean water, providing affordable and clean energy, fostering economic growth, enhancing resource efficiency, reducing waterborne diseases, reducing the burden of water collection, enhancing water management practices, and enhancing water treatment.

1. Introduction

Water is one of humankind's essential natural resources for various domestic and industrial applications. Large quantities of water are used in industries to manufacture different products. Water utilization is increasing daily, which drives people to reuse wastewater containing physical substances and organic contaminants. These modern-day wastewaters contain an overwhelming amount of metals. Heavy metals including copper, lead, zinc, and magnesium surround us, and the intake of these metals in small amounts has long-term impacts.[1] High concentrations of these metals in water impart toxic properties that cause health issues.[2–6] The most commonly discovered substantial metals in wastewater are arsenic, cadmium, chromium, copper, zinc, iron, and lead, which harm human well-being and the environment.[7] Various methodologies have been contemplated to advance cost-effective filtration methods to separate these metals. Significant advancements have been made to reduce the volume of wastewater produced and improve the quality of the treated wastewater.

In recent decades, membrane separation has become a proven technique with remarkable performance, and

[a]Membrane Research Laboratory, Department of Chemical Engineering, National Institute of Technology, Tiruchirappalli 620015, Tamil Nadu, India. E-mail: arthanaree10@yahoo.com; Fax: +91431-2500133; Tel: +91431-2503118

[b]Membrane Research Laboratory, Department of Chemical Engineering, National Institute of Technology Andhra Pradesh, Tadepalligudem 534101, Andhra Pradesh, India

[c]Department of Nanobiotechnology, Faculty of Agricultural Technology, VNU-University of Engineering and Technology, Hanoi 122000, Vietnam

[d]Polymer Science Program, Division of Physical Science, Faculty of Science, Prince of Songkla University, Hat-Yai, Songkhla 90110, Thailand

commercial membrane markets have been spreading rapidly worldwide. Membrane separation has been progressively utilized to treat inorganic waste because of its high effectiveness and low cost. There are diverse membrane filtration methods, such as ultrafiltration (UF), nanofiltration (NF), microfiltration (MF), and reverse osmosis (RO).[8] Membranes have been increasingly used in the treatment of profluents abundant in heavy metals. Membrane in film forms (UF, MF, NF, and RO) were then utilized with different adequacies and selectivities.[9] In particular, cellulose acetate (CA), a biopolymer membrane, is one of the most commonly used membranes owing to its high hydrophilicity, superior mechanical strength, and excellent film-forming capability during fabrication.[10]

Ionic liquids (ILs) have tremendous advantages because of their unique properties, such as low volatility, tuneable consistency, organic solvents, and their great extractability for different natural mixes and metal particles, chiefly relying on their uncommon structures. Ionic liquids are principally utilized for gas separations, and since the previous decade, ILs have likewise been used for heavy metal treatment.[11] The ILs display a dual nature when in salt form; it was found that the expulsion rate and limitations of quaternary ammonium and phosphonium-based ILs associated with wastewater have led to slime formation. In a previous study, the ILs were utilized as the sorbing (extraction) agent to improve the rejection rate of heavy metals. The examined ILs displayed astounding sorbing properties for Zn, Ni, Cu, Cr, Cd, and Pb from actuated wastewater.[12] The metal ion transfer mechanism in ILs and the ionic nature of these ILs can result in different extraction mechanisms, including ion exchange, solvent ion-pair extraction, and a combination of both.[13] William *et al.* have reported that room-temperature ionic liquids consist of the 1-ethyl-3-methylimidazolium (EMIM) cation and bis[(trifluoromethyl)sulfonyl] imide anion and stabilize monomeric ligand-deficient transition-metal complexes (ruthenium, iron and titanium) *via* 4 different modes of binding: monodentate O or N coordination and bidentate N–O or O–O interaction.[13]

In this work, amino acid (AA) and ILs incorporated CA membranes are fabricated using the phase inversion technique for metal separation. The principle of the present work is to expel the metal ions and deduce the concentration of iron (Fe), copper (Cu), lead (Pb), and zinc (Zn) from industrial wastewater using the synthesized AA–IL composite membranes through nanofiltration.

2. Materials and methods

2.1. Materials

The CA polymer and *N,N*-dimethylformamide (DMF) were procured from Merck (India) Ltd, and 1 ethyl 3 methyl-imidazolium chloride was purchased from Tokyo Chemicals, Japan. Amino Acids (AAs), copper sulphate pentahydrate, and magnesium sulphate heptahydrate were purchased from SRL Pvt. Ltd, India. All chemicals used were analytical grade. Ultrapure water is obtained using the Millipore pilot plant.

2.2. Fabrication of amino acid and ionic liquid-incorporated CA membranes

The neat CA and amino acid and ionic liquid-incorporated composite CA membranes were synthesized using the phase inversion-induced immersion precipitation.[14] A schematic representation of the fabrication of the CA/AA/IL membrane is shown in Fig. 1. The compositions of the casting solutions for all the fabricated membranes are given in Table 1. AA, ILs, and AA–IL loading percentages were kept at 0.5%, 1%, and 5% of CA, respectively. AA, IL, and AA–IL were added to DMF, and through sonication, it was dispersed for 1 h using an ultrasonicator to enhance the solution homogeneity. After homogenisation, the CA powder was dissolved in the DMF solution for 4 h by mechanical stirring. Then, the dope solution was subjected to ultrasonication for 30 min to form a complete dispersion of AA and IL. The air bubbles were removed from the casting solution and were cast onto a glass plate, which was finely leveled with a casting knife of 400 μm thickness. Eventually, the thin film is dipped in distilled water and kept at 10 °C to ensure complete phase inversion.[15] The membranes are
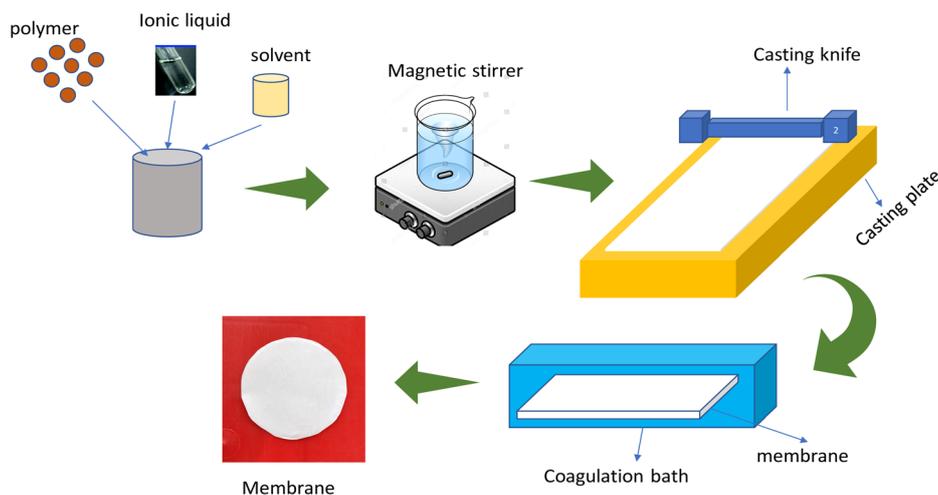

Fig. 1 Fabrication of the membranes.

Table 1 Composition of casting solutions

| Membrane code | CA, AA and IL composition (17.5 wt%) | | | Solvent (wt%) |
	CA	AA	IL	DMF
M1	100%	—	—	82.5%
M2	99%	1%	—	82.5%
M3	94%	1%	5%	82.5%
M4	99%	0.5%	0.5%	82.5%

named as follows: neat CA membrane as M1, CA-(1%) of AA as M2, CA-(5%) of IL, (1%) of AA as M3, CA-(0.5%) of AA as M4.

2.3. Characterisation of membranes

2.3.1. Fourier transform infrared (FTIR) spectroscopy. The change in the chemical structure and AA–IL functional groups was analysed using an ATR-interfaced Fourier transform infrared (FTIR) spectrophotometer (Thermo Scientific Nicolet iS5 FT-IR spectrometer). The change in chemical structure can be observed by the wavenumber drift against the percentage transmittance for the samples collected over the spectral region of wavelengths from 400 to 4000 cm^{-1}.[16]

2.3.2. Thermogravimetric analysis. The thermal stability of the prepared neat CA and AA, IL incorporated CA membranes were examined using a thermogravimetric analyser (DGT 2000, PerkinElmer, 2915 133rd Street West, USA). All the fabricated membrane samples were allowed to dry in a vacuum oven at 60 °C for 24 h before testing. The prepared membrane samples were analysed with a heating rate of 10 °C min^{-1} from 50 to 700 °C under a nitrogen atmosphere.[11]

2.3.3. Differential scanning calorimetry. DSC is used to quantify the changes in heat flows related to material changes. The DSC estimation provides both quantitative and subjective information on endothermic and exothermic forms. DSC is commonly used to determine the glass transition temperature and melting point of crystalline polymeric materials. All the fabricated membrane samples were dried in a vacuum oven at 60 °C. The samples were analysed from 50–700 °C at a heating rate of 10 °C min^{-1} under nitrogen air.[17]

2.3.4. Surface morphology. The neat CA and composite CA, AA, and IL membrane cross-sections were scanned with a scanning electron microscope (SEM) and an energy-dispersive X-ray spectroscope (VEGA 3, TESCAN, USA). The cross-sectional image of the neat CA, AA, and IL membranes was obtained by keeping the samples in the cathode field emission at 1–15 kV. Before taking the cross-sectional images, all the fabricated membrane samples were frozen in liquid nitrogen and fractured. The prepared membrane samples were cut into required pieces, cleaned with filter paper, and kept in an air drier. The dried pieces of membrane samples were varnished with gold by bubbling to make them conductive.

2.3.5. Surface topology of fabricated membranes. Atomic force microscopy (AFM) is used to identify the surface roughness parameter by the tapping mode method (Nano surf Scanning Probe Optical Microscope, easy scan II, USA).[18]

2.3.6. Membrane porosity and pore size. All the fabricated samples were cut into specific sizes and then mopped with filter paper. After obtaining the wet weight, the samples were allowed to dry in a vacuum oven at 60 °C for one day. The porosity (ε) is determined from the dry and wet weights of the membranes using the following equation [eqn (1)].[19]

$$\varepsilon = \left(\frac{\dfrac{\omega_1 - \omega_2}{d_w}}{\dfrac{(\omega_1 - \omega_2)}{d_w} + \left(\dfrac{\omega_2}{d_p}\right)} \right) \tag{1}$$

ω_1 – the wet weight of the fabricated membrane sample (g), ω_2 – the dry weight of the fabricated membrane sample (g), d_w – water density (kg cm^{-3}), d_p – polymer density (kg cm^{-3}).

Using the filtration velocity technique, the mean radius of the fabricated membrane pore was calculated using the Guiraud–Elford–Ferry (GEF) equation [eqn (2)].[20]

$$r_m = \sqrt{\left(\frac{(2.9 - 1.75\varepsilon)8Ql\eta}{\varepsilon A \Delta P} \right)} \tag{2}$$

Q – flow rate of the permeate (m^3 s^{-1}), A – effective cross-sectional area of the membrane (m^2), ΔP – transmembrane pressure (Pa), η – dynamic viscosity of water (Pa s), l – thickness of the membrane (m).

2.3.7. Contact angle measurement. The hydrophilicity of neat CA, AA, and IL-incorporated composite CA membranes was examined using the contact angle measurement. The goniometer (demonstrate rame-hart 250-F1, USA) was used for contact angle measurements using the sessile drop technique for the fabricated membranes. About 5 μL distilled water drop is infused on the top surface of a dry membrane at five unique areas using a micro syringe. The contact angle value was estimated from the independent distilled water droplets in the five different regions, which decide the hydrophilicity of the layer.

2.4. Work of adhesion

The work of adhesion (ΔG_S) is called the surface free energy. This assesses the firmness of the contact between the membrane and surface water. W_a is the amount of work needed to segregate two different liquid–solid or liquid–liquid boundary phases from each other.[14]

W_a is calculated from the Young's equation using the contact angle [eqn (3)].

$$-\Delta G_S = (1 + \cos \propto)\gamma \tag{3}$$

where, $\propto$ is the contact angle of the sample and γ represents the water surface tension (72.8 mJ m^{-2}).

2.5. Hydration capacity

Hydration capacity was calculated by the difference in the wet weight (a membrane immersed in distilled water at 30 °C for 1 day) and dry weight of the fabricated membrane, thickness and total surface area of the membrane [eqn (4)].

$$\text{Hydration capacity} = \frac{W_w - W_d}{A \times l} \, (\text{mJ/m}^2) \tag{4}$$

Fig. 2 Nanofiltration experimental set-up.

2.6. Permeation studies

The nanofiltration experiment was conducted for pure water flux and heavy metal solution with the pressure of 4 bar, with nitrogen gas as a pressure-developing medium using neat CA membrane (M1) and AA, IL incorporated CA membranes (M2, M3, and M4). The permeation of neat CA and AA, ILs incorporated composite membranes were studied for pure water and heavy metal solutions at 4 bar pressure and pH 7 using a dead-end nanofiltration cell (model HP4750 STIRRED CELL, AVENUE S KENT, USA), as shown in Fig. 2, and an effective membrane area of 14.6 cm^2. Initially, membrane compaction was done to collect the steady-state permeates. Once a steady state was observed, the permeate was collected for a period of time for each membrane. The flux (J_w) of the membrane was calculated using the equation [eqn (5)].[1]

$$J_w = \frac{V}{A \times \Delta t} \qquad (5)$$

where, J_w = pure water flux (L m^{-2} h^{-1}), V = permeating volume (L), A = effective membrane area (m^2), and Δt = permeation time (h).

2.6.1. Permeation and rejection performance at different operating conditions. The changes in permeate fluxes and pure water flux were studied by varying the pressure. Also, the rejection rates of magnesium and copper for these fabricated membranes were scrutinized with synthetic wastewater using nanofiltration. The experiment was conducted under three different operating pressures: 2, 4, and 6 MPa, with a pH of 4 and 7, as these factors are critical in influencing the permeate flux, rejection efficiency, solution chemistry, and the membrane's surface charge.[21] All the experiments were conducted in triplicate.

2.7. Treatment of wastewater from a metal ion-based industry

The wastewater utilized in the process was procured from a metal industry in Tiruchirappalli, Tamil Nadu, India. The composition and characteristics of wastewater are presented in Table 2. The concentration of heavy metals was tested using atomic absorption spectroscopy (Systronics Limited, India).

Table 2 Characteristics of wastewater

Parameters	Values
pH	6.6
TDS (ppm)	176
COD (ppm)	1580
Turbidity (NTU)	20.8
Iron (ppm)	6.65
Copper (ppm)	3.40
Lead (ppm)	4.37
Zinc (ppm)	5.19

Table 2 shows that industrial wastewater generally has higher concentrations of iron, copper, lead, and zinc particles than other cations.[6] The rejection percentage of industrial wastewater for both neat CA and CA, AA, IL membranes was evaluated by the following equation [eqn (6)].

$$R = \left(1 - \frac{C_f}{C_p}\right) \times 100 \qquad (6)$$

C_f – feed concentrations of the heavy metal solutions and C_p – permeate concentrations of the heavy metal solutions.

3. Results and discussions

3.1. Confirmation of AA, IL in polymer membrane

The FTIR spectra of the neat CA (M1), amino acid, and ionic liquid grafted membranes with different compositions (M2, M3, and M4) are shown in Fig. 3. The major absorbance bands are observed at 3400 cm^{-1}, corresponding to the OH group stretching vibration. Compared to the neat membrane, new characteristic peaks of the CA–AA membranes at 3388 cm^{-1} correspond to the stretching vibration of N–H, which indicates that the amino acid salt has been successfully incorporated into the neat CA membrane. The band at 450 cm^{-1} is from the alkyl halide of IL, confirming the presence of IL. Similarly, no specific changes were observed in the spectra when AA–IL is grafted onto the surface of neat CA, *i.e.*, due to the neat CA having functional groups similar to the CA–IL–AA membrane. The peaks observed at 2892 cm^{-1} have been reported to be anti-symmetric CH$_3$ stretching due to the presence of the imidazolium part of ILs.[22]

3.2. Surface morphology of the fabricated membrane

Fig. 4 and 5 identify the morphological structure in all fabricated membranes. The neat CA membrane's surface morphology is smooth and has a non-porous structure. The CA–AA surface is totally rough when compared to that of the neat membrane due to the presence of amino acids, where complete dispersion was observed along with voids. The (CA–AA–IL-5%) membrane and (CA–AA–IL-0.5%) surfaces have flattened shapes and appear to have rough surfaces along with micropores.

Fig. 5 shows the cross-sectional morphology with an asymmetric structure. The neat CA membrane shows the presence of macro voids with a thick skin layer on the top. The presence of large finger-like structures with a decrease in the thickness of
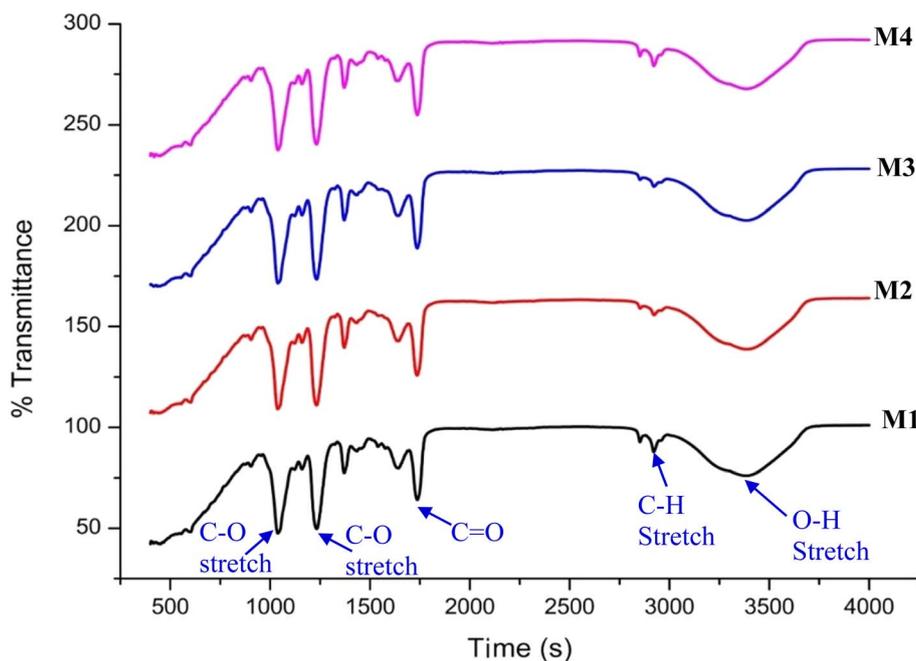
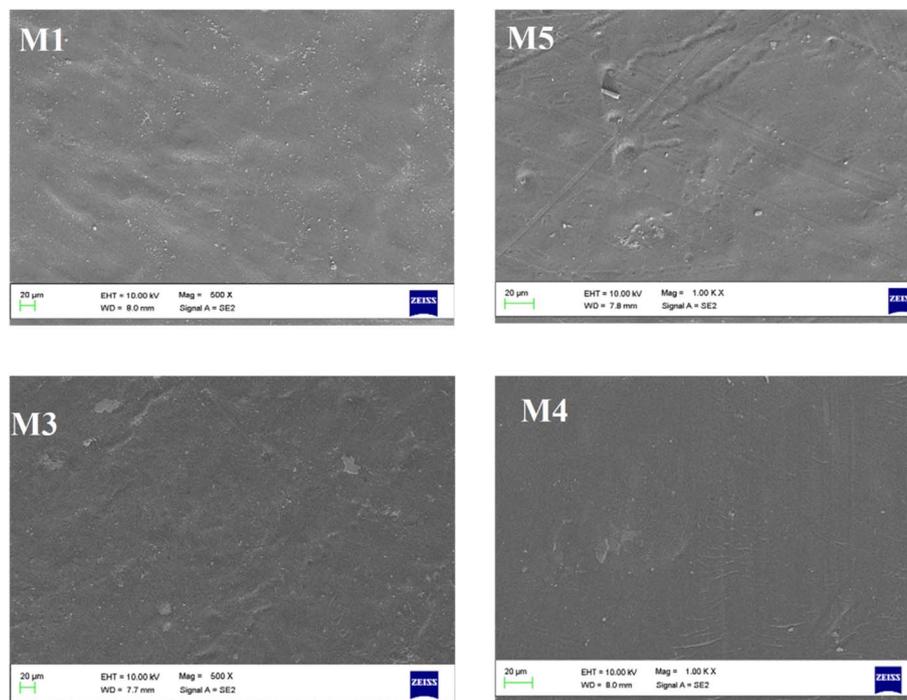Fig. 3   FTIR spectra of the fabricated membranes.

Fig. 4   Surface morphology of the fabricated membranes.

the skin layer is due to the addition of AA. Adding ionic liquid and amino acid to the CA membrane with two different compositions shows the increase of macro voids due to the increased ionic liquid percentage, which decreases the surface skin layer from a dense layer to a thin layer (Fig. 5). The primary role of IL additives is to increase the membrane's hydrophilicity.[22]

3.3.   Surface topology of the fabricated membrane

Fig. 6 shows the AFM images of CA, CA/AA, and CA/IL membranes obtained by the tapping mode. The neat membrane appeared to be rough on the surface, with many small craters and valley structures. The neat CA membrane also showed high hydrophilicity, as evidenced by a contact angle of
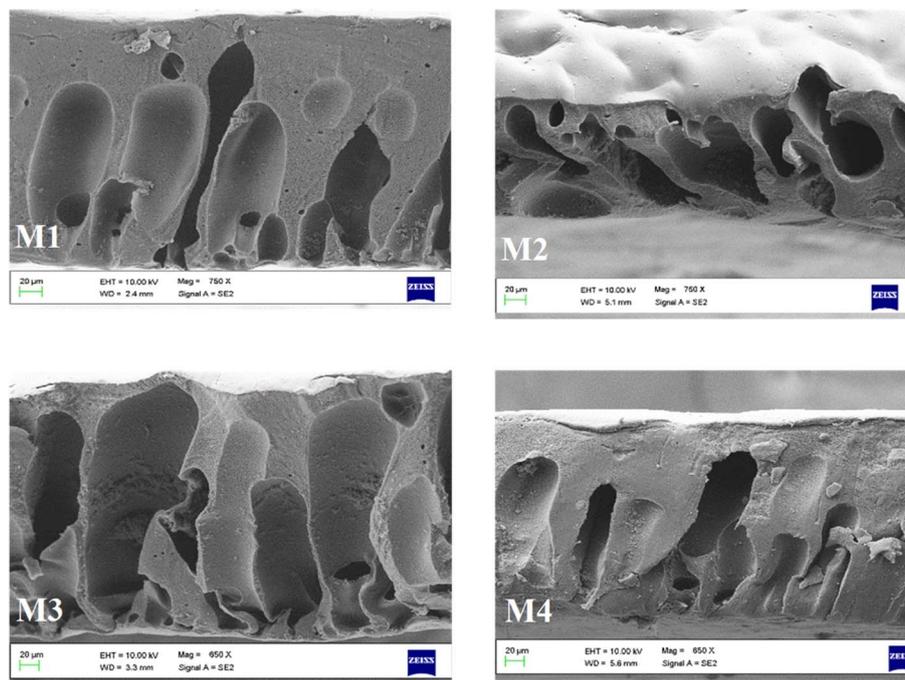
Fig. 5 Cross-sectional morphology of the fabricated membranes.

51.18°, which contributes to its higher water flux.[23] The AA-embedded polymeric membrane was observed to have a smooth and flat surface with a decrease in the crater valley surface compared to the neat CA membrane. The depletion in the roughness of the membranes was clearly due to the doping of AA into the neat CA.[22] This smoothing effect resulted in
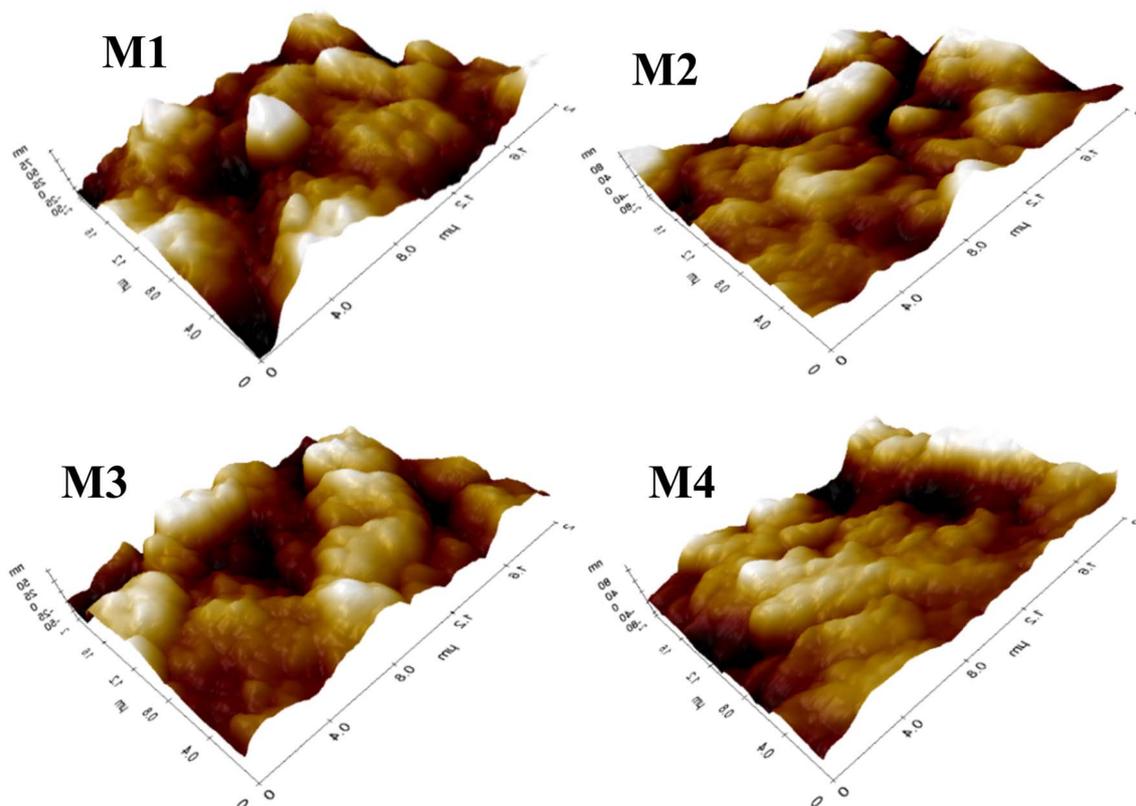

Fig. 6 Surface topology of the fabricated membranes.

a higher hydrophobicity of membrane M2, as indicated by a contact angle of 68.39°. On the other hand, the incorporation of IL into membrane M3 resulted in a rougher surface, which enhanced the hydrophilicity, as supported by the contact angle of 51.94°.[24]

3.4. Contact angle measurement

Table 3 shows the contact angles of the fabricated membranes (Fig. 7). The neat CA membrane has a contact angle of 51.18°. When compared to the neat CA membrane, the contact angle of the amino acid incorporated membrane was increased to 68.39°. This is due to the Rose Petal Effect (The microstructure controls the contact angle hysteresis, whereas the nanostructure provides high CA. As a result, a rose petal can exhibit typical lotus effect properties (high CA and low CA hysteresis) or petal effect properties (high CA and high CA hysteresis)). Artificial surfaces that mimic rose petals were investigated, and similar behavior was found,[25] which explains the hydrophobicity of amino acids; in the case of CA–AA–ILs membranes, the contact angles have been increased to 63.06°, and this might be due to the presence of the amino acid group, *i.e.*, contact angle tends to increase as the pH varies from alkaline to acidic. The

composite membrane became hydrophilic because of the increase in the loading of 5% chlorine-based ionic liquid. This could be credited to the hydrophilic nature of the chlorine-based ionic liquid.[26] At higher concentrations of the ionic liquid, the decrease in contact angle enhances the membrane hydrophilicity, forming a stable hydration layer over the surface. This hydration layer acts as a protective barrier, repelling foulants, such as proteins, bacteria, and organic matter, by preventing their direct adhesion. The presence of a well-structured hydration layer reduces the surface energy and minimizes hydrophobic interactions, thereby improving the antifouling efficiency.[27] The increase in contact angle due to the incorporation of amino acids demonstrates the hydrophobicity of membranes. Halan *et al.* reported a similar effect of charge and hydrophilicity on the antifouling properties of polyester membranes.[28] Thus, the synergistic effect of amino acids and ionic liquids not only modifies the membrane's surface wettability but also improves its antifouling properties, making it more resistant to both organic and inorganic foulants.

3.5. Thermo gravimetric analysis

The thermal properties of the membranes were determined using thermogravimetric analysis (TGA), as shown in Fig. 8. All the fabricated membranes have better thermal stability up to 330 °C. The weight loss is 4% up to 330 °C for the neat membrane (M1). Adding ionic liquid and amino acid influences the membranes' thermal stability. The other membrane, M2, has a slightly lower weight loss percentage (3%) than the neat membrane (M1), indicating improved thermal stability.

The membranes M3 (CA–AA–IL-5%) and M4 (CA–AA–IL-0.5%) have less thermal stability because of chloride ions within

Table 3 Contact angles of the fabricated membranes

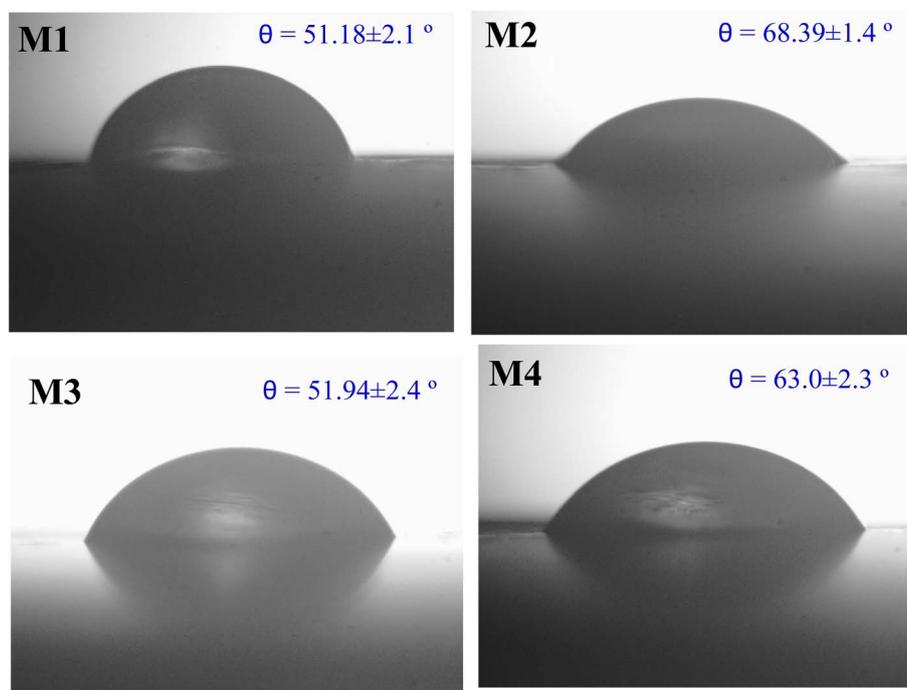| Membrane	Name of the membranes	Water contact angle (°)
M1	Neat CA	51.18 ± 2.1
M2	CA + AA (1%)	68.39 ± 1.4
M3	CA + AA (1%) + IL (5%)	51.94 ± 2.4
M4	CA + AA (0.5%) + IL (0.5%)	63.0 ± 2.3

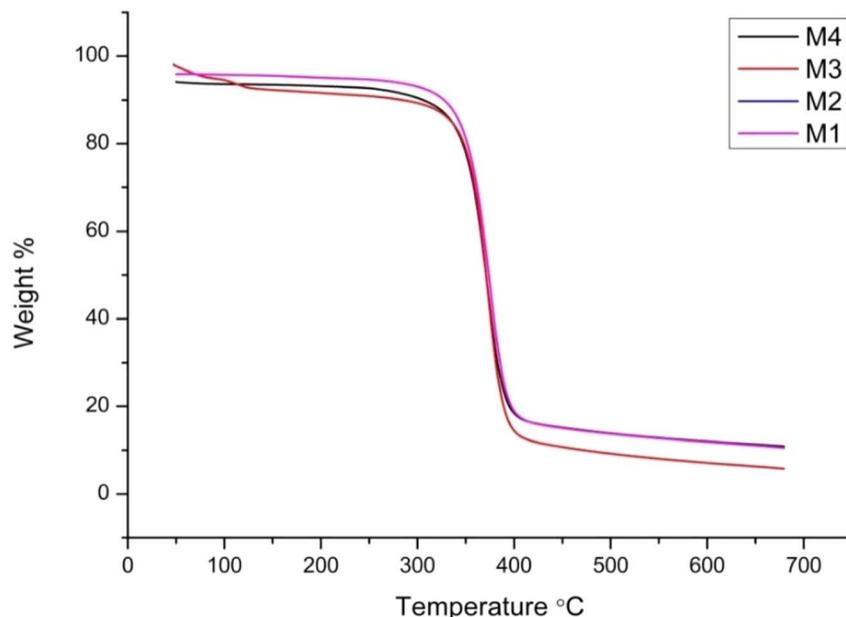**Fig. 7** Contact angle images of the fabricated membranes.

Fig. 8   TGA analysis of the membranes.

the membrane matrix and tend to degrade with a weight loss of 6% up to 145 °C. Subsequently, CA–AA is stable up to 330 °C due to the presence of amino acids, and the degradation from 330 °C is due to the CA membrane.[23] The observed thermal stability enhancements suggest that the interactions between amino acids and the CA matrix improve the polymer chain rigidity, thereby delaying thermal degradation.[29] Additionally, the ionic liquid incorporation influences the membrane decomposition behavior, which aligns with the findings of Lea Chancelier. The impact of the alkyl chain length and the presence of functional groups and unsaturation were evaluated, revealing that the thermal behavior is governed by the van der Waals interactions between the alkyl chains and inter- and intra-molecular coulombic interactions, such as hydrogen bonding.[30]

3.6.   Differential scanning calorimetry

DSC is a technique where thermal analysis is carried out to measure the heat flow changes related to material transitions. Fig. 9 shows that all membranes have exothermic peaks on the thermogram associated with the melting of the membrane
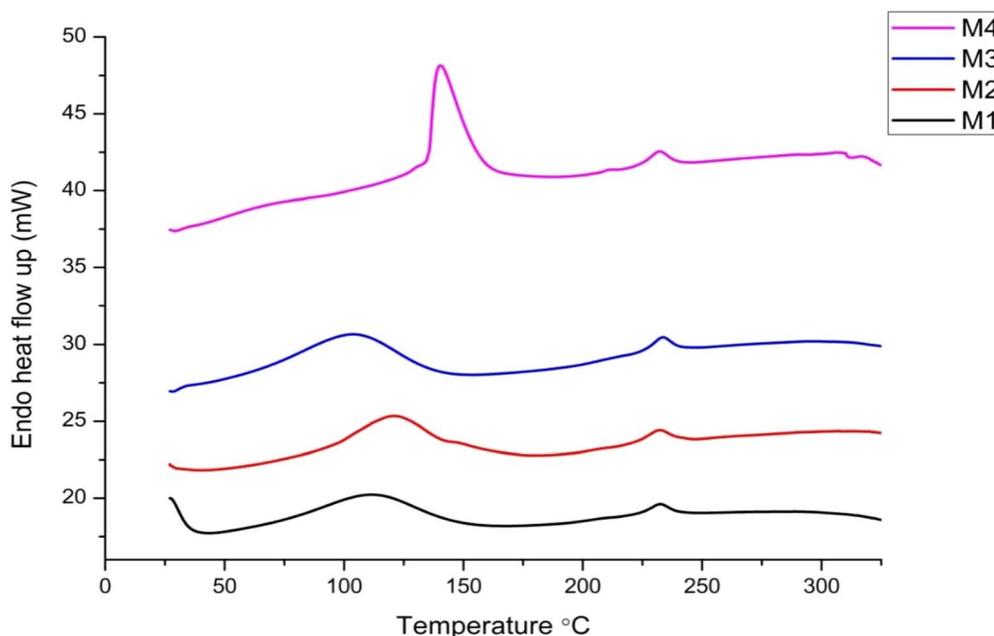

Fig. 9   DSC analysis of the membranes.

samples. The T_g value of neat CA was observed to be 64 °C, whereas the T_g of the amino acid incorporated membrane CA–AA is 91 °C, indicating enhanced thermal stability. This increase in T_g is attributed to strong interactions between the amino acid molecules and the CA polymer matrix. Additionally, the DSC results further validate the TGA findings, as the improved thermal stability of modified membranes correlates with increased T_g values.

It could be expected that a decrease in the concentration of ionic liquid, as explained by Lea Chancelier,[20] will lead to a reduction in the melting point of the membrane. (CA–AA–IL-5%) has a higher melting point compared to that of (CA–AA–IL-0.5%), which suggests that a higher ionic liquid concentration influences the intermolecular interactions and phase transitions. This correlation between thermal stability,

decomposition behavior, and glass transition temperature further supports the structural modifications induced by the amino acid and ionic liquid incorporation, demonstrating their influence on the membrane's thermal properties.

3.7. Pore size and porosity of membranes

The porosity of the (CA–AA–IL-5%) incorporated CA membrane increases from 36.42 to 44.15% with the increasing concentration of ILs in the CA membranes from 0 to 5%. The increasing porosity of the membranes impacts the membrane flux.[31] The pore size of the membranes is gradually rising from 3.16 to 3.91 nm with the increasing concentration of the AA, IL from 0 to 5% in the CA membrane, as shown in Table 4. The membrane pores have a positive charge due to the incorporation of ionic liquid, which reduces the viscosity of wastewater, allowing it to pass freely. Consequently, the permeate flux increases. The formation of pores in the membrane surface enhances the permeability of membranes.[18] For the (CA–AA–IL-0.5%) incorporated CA membrane, the translocation of hydrophobic amino acids may involve a modest amount of partitioning into the membrane interior, as well as translocation through transient defects; as a result, small pores were formed, which increases the rejection rate.

Table 4 Pore size of the fabricated membranes

Membrane	Pore size (nm)
M1	0.0291
M2	0.0136
M3	0.0316
M4	0.0110

Table 5 Flux of pure water and metal ion solution at pH 7 and 4 bar pressure

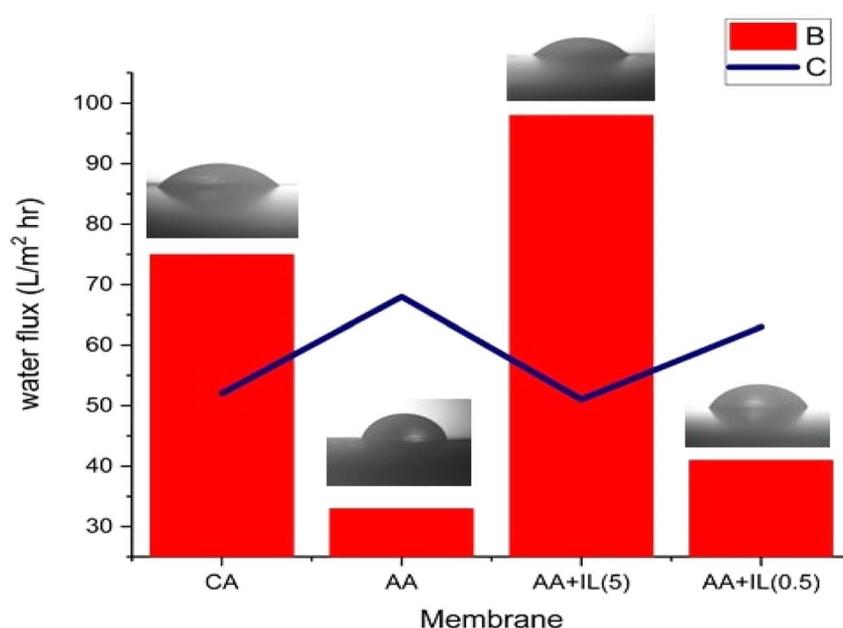| Membrane	Pure water flux ($L\ m^{-2}\ h^{-1}$)	Heavy metal solution flux of copper ($L\ m^{-2}\ h^{-1}$)	Heavy metal solution flux of magnesium ($L\ m^{-2}\ h^{-1}$)
M1	75.13	62	77
M2	32.87	15	12
M3	98.60	73	70
M4	41.09	10	12

Fig. 10 Pure water flux of membranes.

3.8. Permeability of membranes

The pure water flux of neat CA and AA–IL membranes is listed in Table 5 (Fig. 10). When applying 4 bar pressure to membranes,

the flux increased from 75 L m^{-2} h^{-1} to 98 L m^{-2} h^{-1}, and the rising concentration of AA influenced the increasing permeability of CA membranes–IL in CA membranes. It confirms that adding AA–IL effectively enhanced the hydrophilicity and pore

(a) NF performance of membranes at a pressure of 2 bar at pH 4

(b) NF performance of membranes at a pressure of 2 bar at pH 7

(c) NF performance of membranes at a pressure of 4 bar at pH 4

(d) NF performance of membranes at a pressure of 4 bar at pH 7

(e) NF performance of membranes at a pressure of 6 bar at pH 4

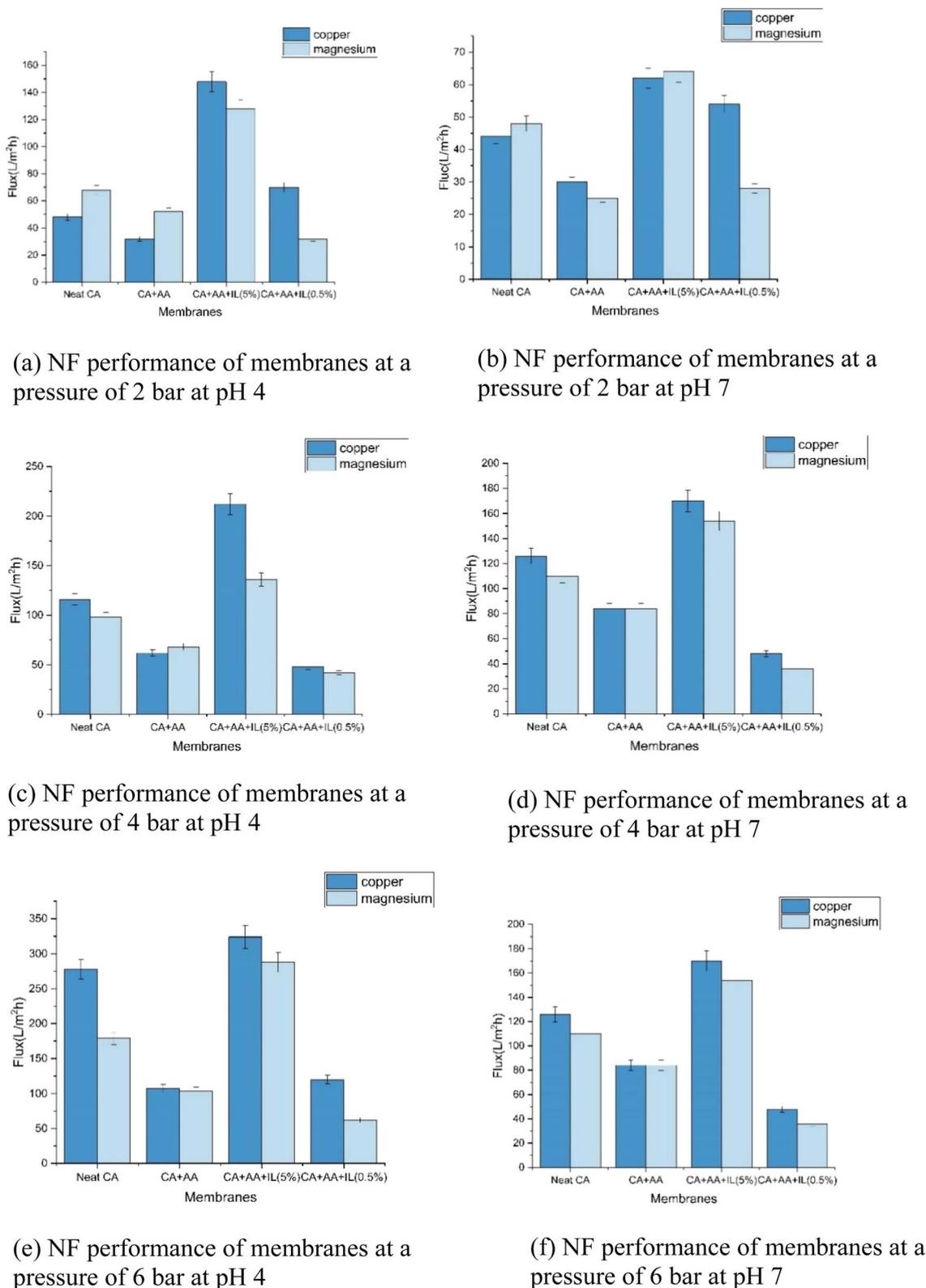(f) NF performance of membranes at a pressure of 6 bar at pH 7

Fig. 11 Flux of metal ion solution for copper and magnesium.

formation of the CA membranes, which is due to the fact that during the A-IL membrane modification, the ILs replace a part of the polymer, regulating the chemical and hydrogen bonding of the CA chains and enhance hydrophilicity and pore formation. However, the mean pore sizes of the CA + AA (1%) + IL (5%) membrane only increase marginally compared to the neat CA membrane. It means the flux improvement happened due to the enhanced hydrophilicity and the possibly larger pore size on the surfaces of the AA–IL membranes, which allows the transport of water through the surface/internal pores more quickly.

The incorporation of amino acids and ionic liquids into cellulose acetate membranes enhances hydrophilicity, leading to improved water flux and antifouling properties.[32] However, increased hydrophilicity can sometimes compromise mechanical strength due to higher water absorption, which may weaken the polymer matrix. Conversely, amino acid incorporation can enhance mechanical stability through hydrogen bonding and

intermolecular interactions, partially mitigating this effect. Thus, optimizing the concentration of these additives is crucial to achieving a balance between high water permeability and sufficient mechanical robustness for long-term applications.

3.9. Nanofiltration performance at different pressures and pH

The NF performance for the copper and magnesium metal ion solutions at different pressures and pH are conducted, and the results are presented in Fig. 11. The operating pressure increases from 2 to 6 bar at a pH of 4 to 7. It was observed that the flux values of both synthetic and real wastewater increased, and the rejection rates decreased. At all operating pressures, copper and magnesium solutions had the highest flux at a pH of 4. The highest flux was 209 L m^{-2} h^{-1} for the (CA–AA–IL-5%) membrane, while 127 L m^{-2} h^{-1} was observed for the neat CA membrane for the copper metal ion solution. It was found to be 152 L m^{-2} h^{-1} for the (CA–AA–IL-5%) membrane while 111 L m^{-2} h^{-1} for the neat CA membrane for the magnesium metal ion solution. A similar type of flux values were found at 4 bar pressure. The highest flux was observed for copper metal ions at 6 bar pressure at pH 4 compared to pH 7. It was observed to be 320 L m^{-2} h^{-1} for the (CA–AA–IL-5%) membrane and 279 L m^{-2} h^{-1} for the neat CA membrane for the copper metal ion solution. The values were 295 L m^{-2} h^{-1} for the (CA–AA–IL-5%) membrane and 189 L m^{-2} h^{-1} for the neat CA membrane for the Mg metal ion solution. It can be seen that all of the pure water flux (PWF) and NF performances have the same variation trend. Fig. 12 gives the flux values of industrial wastewater. Compared with the neat membrane, the ionic liquid (5%) and amino acid (1%) incorporated membrane have higher flux values than the neat membrane due to the hydrophilic nature of the IL-embedded membrane. The flux of (CA–AA–IL-5%) was very high, 78 (L m^{-2} h^{-1}), because of the chloride-based ionic liquid. The (CA–AA–IL-0.5%) membrane had a very low flux of 33 (L m^{-2} h^{-1}) compared to that of (CA–AA–IL-0.5%) because of
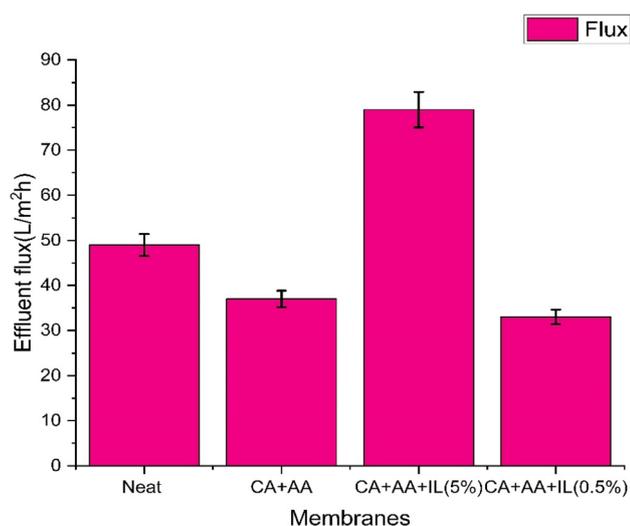

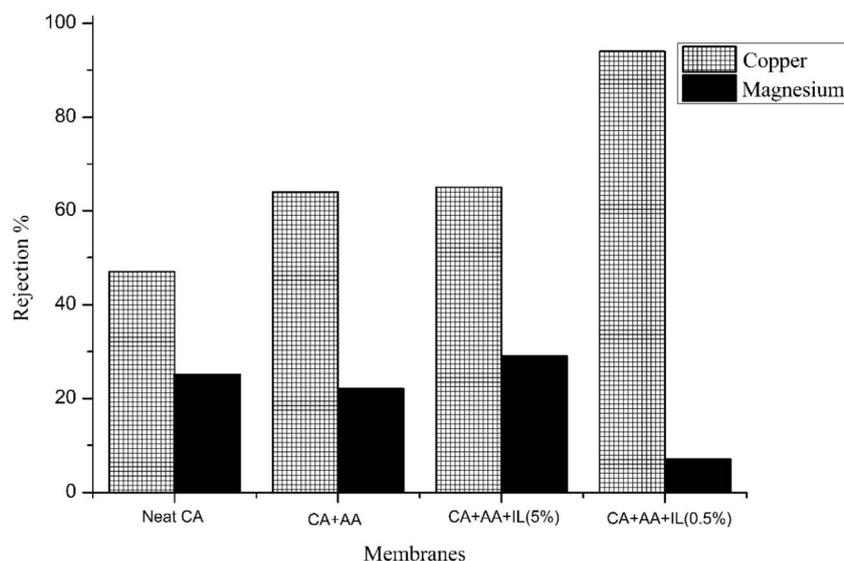**Fig. 12** Nanofiltration performance of industrial wastewater.

Fig. 13 Rejection percentage of the metal ion solution for copper and magnesium.

© 2025 The Author(s). Published by the Royal Society of Chemistry

lower values of IL compared to other membranes. It is observed that the pure water and permeate flux for industrial wastewater treatment increases directly when the operating pressure increases.

Consequently, the flux values decrease as the pH increases. A similar change was observed elsewhere.[1,31] Fig. 11 shows that increased operating pressure results in overcoming the resistance of the membrane and enhancing the driving force.
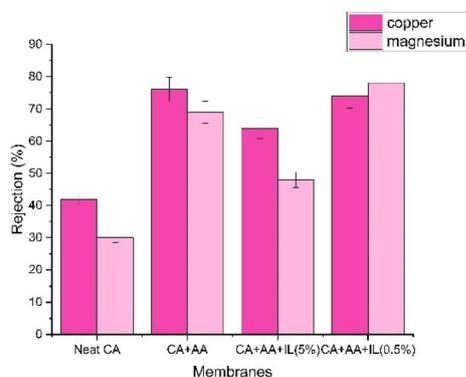
(a) Rejection performance of the membranes at a pressure of 2 bar at pH 4
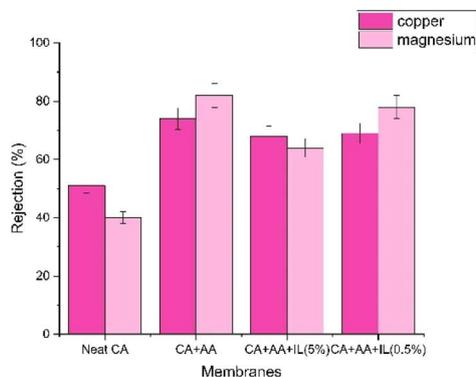
(b) Rejection performance of the membranes at a pressure of 2 bar at pH 7
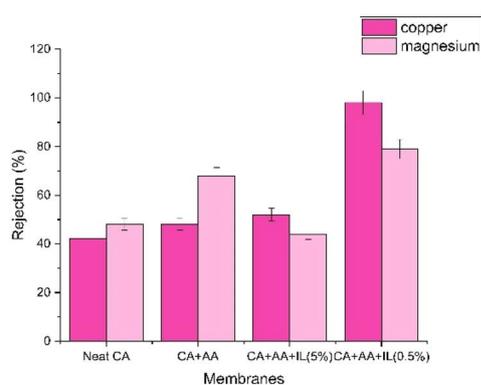
(c) Rejection performance of the membranes at a pressure of 4 bar at pH 4

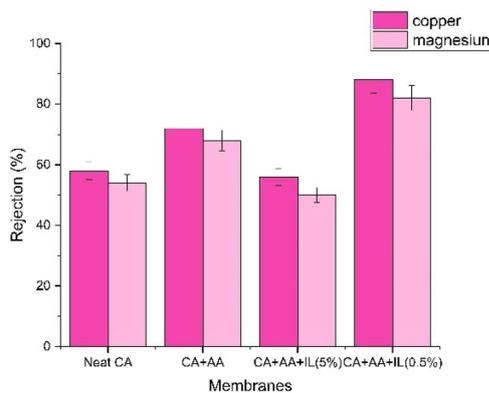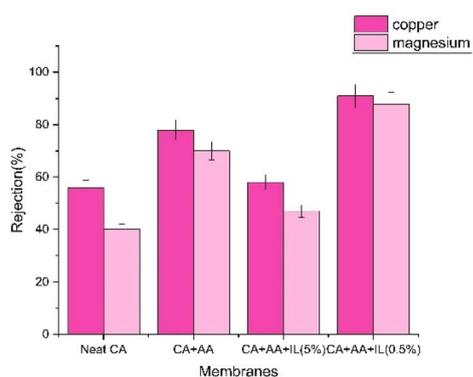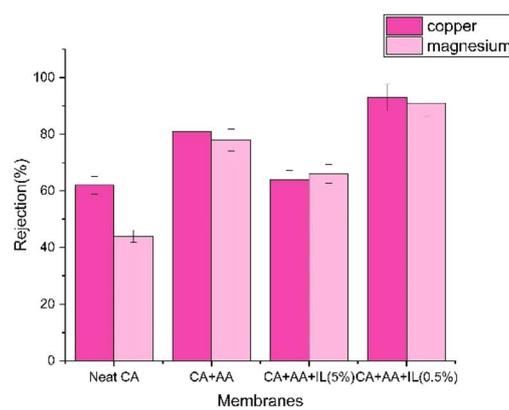(d) Rejection performance of the membranes at a pressure of 4 bar at pH 7

(e) Rejection performance of the membranes at a pressure of 6 bar at pH 4

(a) Rejection performance of the membranes at a pressure of 6 bar at pH 7

Fig. 14 Rejection percentage of metal ion solution for copper and magnesium at different pressures and pH.

Besides, the difference between the permeate and pure water flux for industrial wastewater treatment increased with the operating pressure because the concentration polarization is negligible under lower operating pressures but not at higher pressures. When the operating pressure increases, the concentration polarization also tends to increase, increasing the osmotic pressure that leads to a decline in the total effective pressure, decreasing the permeate flux, and increasing rejection rates.[33] In conditions of low pressure, surface forces become more significant than training forces. Additionally, as pressure rises, solvent flux also increases, which leads to a decrease in permeate solute concentration by raising its rejection rate. After certain pressure levels, the surface forces of the solute become weak compared to the training forces; thus, the transportation increases in the solute and reduces the rejection rates.[34]

3.10. Effluent rejection

The rejection performance of these fabricated membranes was studied using a synthetic metal ion solution for Cu and Mg (1000 ppm) by varying the pressure and pH for industrial wastewater. The studies were conducted at a pressure of 4 bar and pH 7 for industrial wastewater, whereas the pressure and pH varied for the synthetic metal ion solution. The results are shown in Table 5 and Fig. 13. The rejection experiments were carried out at pH 7. A higher Cu, Zn rejection% of 90%, 91% was observed for the (CA–AA–IL-5%) membrane when compared to all other membranes; this might be due to the low pore size and surface blocks, rejecting the metal ions passing through the surface. A higher rejection was observed at pH 7 for the AA-embedded polymeric membrane, *i.e.*, 82%, which is explained by the membrane's pore-size modification mechanisms and SEM images. Additionally, the Donnan exclusion effect plays a critical role, where the fixed charged groups on the membrane surface induce electrostatic repulsion with co-ions.[35] This electrostatic repulsion effect is particularly pronounced for multivalent metal ions, contributing to the observed higher rejection rates for copper and zinc compared to magnesium or iron. The highest rejection was observed for copper at 4 bar pressure at pH 7 compared to that at pH 4. It was observed to be 88% for the (CA–AA–IL-0.5%) embedded polymeric membrane and 58% for the neat CA membrane for the copper solution at a pH of 7. The rejection rate was 83% for the (CA–AA–IL-0.5%) embedded polymeric membrane while 54% for the neat CA membrane for the magnesium metal ion solution. The highest rejection was observed for copper at 6 bar pressure at pH 7 compared to that at pH 4. It was observed to be 93% for the (CA–AA–IL-0.5%) embedded polymeric membrane, while 62% for the neat CA membrane for the copper solution at a pH of 7. It was observed to be 89% for the (CA–AA–IL-5%) embedded polymeric membrane and 44% for the neat CA membrane for magnesium metal ion solution at a pH of 7. Consequently, as the pH changes from pH 4 to 7, the membrane pore size has a reduced positive charge, and as a result, there is a decline in the permeate flux, which leads to a gradual increase in the rejection rate of metal ion solution. It is observed that the rejection performance slowly increases with a rise in pH; higher rejection values were seen for pH 7 on average.

The operating pressure influence on the magnesium and copper rejection rates using the fabricated membranes from industrial wastewater is shown in Fig. 14. As the operating pressure increases, there is an increase in the rejection rates of all heavy metals, which can be explained as follows: the low rejection rate was observed due to low operating pressure; higher diffusive transport can be observed than convective transport through the membranes. Convective transport becomes more prominent compared to diffusive transport, which reduces the solute concentration in the permeate, resulting in a hike in the rejection rate of the solute;[36] however, as the operating pressure increases, concentration polarization also tends to increase, which leads to a decline in the solute dismissal rates by a reduction in the charge impact. The subsequent improved heavy metal rejection rates with increasing operating pressure demonstrate that the increase in convective transport dominates the solute rejection behavior at all operating pressures. According to the Donnan exclusion principle, more rejection rates are observed for heavy metals with high valence charges due to the stronger electrostatic repulsion exerted by the membrane.[37] Therefore, copper and zinc rejection rates are higher than that of the remaining metal ions.

Rejection studies were carried out for industrial wastewater using a nanofiltration setup with all four different fabricated membranes at a pressure of 4 bar and pH. The rejection rates for the 4 different metals are shown in Table 6. The highest rejection rate for iron was 89% for the (CA–AA–IL-0.5%) membrane compared to other membranes. The highest rejection rate for zinc was 91% for both CA–AA and (CA–AA–IL-0.5%) membranes compared to the other two membranes. The highest rejection rate for lead was found to be 84% for the (CA–AA–IL-0.5%) membrane compared to other membranes. The highest rejection rate for copper was found to be 90% for the (CA–AA–IL-0.5%) membrane compared to other membranes. Notably, there is a 90% rejection when the adhesion strength between copper and the polymer creates a strong and reliable connection.[38] The obtained rejection rates of heavy metal ions were comparable to those reported in other research studies. For instance, a metal–organic framework-embedded CA membrane achieved rejection rates of 77% for Co(II) and 53% for Cu(II).[39] Similarly, CA membranes produced from cigarette butt recycling demonstrated rejection efficiencies of 85.2%, 88.4%, and 85.3% for lead, chromium, and cadmium, respectively.[40] Additionally, another study reported the removal efficiencies of Fe^{2+}, Ba^{2+}, and Al^{3+} from dam water using CA membranes as 91.95%, 83.33%, and 59.37%, respectively.[41] These comparisons highlight the competitive performance of the fabricated membranes in heavy metal removal.

Table 6 Rejection % of metals present in industrial wastewater

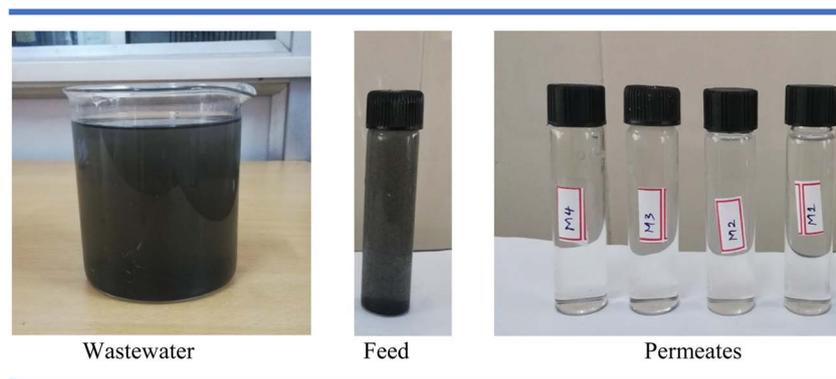| Membrane	Iron (%)	Zinc (%)	Lead (%)	Copper (%)
M1	83	71	64	73
M2	81	91	84	80
M3	83	67	76	79
M4	89	91	84	90

Fig. 15 Feed and permeate of wastewater.

A pictorial representation of the feed and permeate samples of the industrial wastewater treatment carried out in this study is presented in Fig. 15. In this study, the incorporation of ILs enhanced the hydrophilicity of the membranes, improving the water flux and antifouling properties. However, excessive hydrophilicity may sometimes impact the mechanical strength and durability of the membranes. By optimizing the concentration of AA and IL, a balance was achieved, ensuring improved permeability while maintaining sufficient structural integrity for effective nanofiltration applications. AA–ILs have also been considered to be environmentally friendly and greener than conventional solvents and have negligible leaching during membrane formation. In addition, the synergistic effect of both AA and ILs can be modulated to selectively remove metal substances, making them useful for the removal of metal ions from effluents. Overall, the combination of AA and ILs has great potential for use in sustainable and efficient metal ion separation processes.

4. Conclusion

The AA–IL incorporated CA membranes were prepared using the phase inversion method in this work. The membranes were characterized by various methods, such as SEM, contact angle, DSC, and TGA. The contact angle disclosed that the wettability of the membranes varied significantly by adding AA and ILs. The surface morphology of the fabricated membranes also varied compared to the neat CA membrane. TGA and DSC exhibited that the thermal stability of the fabricated membranes was altered due to the addition of AA–IL. The AA–IL enhanced the hydrophilicity, which is confirmed by the contact angles of the membranes and also by pure water flux values. Further, nanofiltration (NF) experiments were conducted to separate heavy metals such as copper, zinc, iron, and lead from industrial wastewater at different pH levels and pressures on the permeate flux, and rejection rates were determined for industrial wastewater. The developed membrane potentially rejected copper, zinc, iron, and lead 89%, 91%, 84%, and 90%, respectively, for 0.5% of AA and IL incorporation. The rejection of heavy metal ions was significantly improved with the inclusion of AA and ILs. Notably, the fabricated membranes

demonstrate promising performance for heavy metal removal while being environmentally friendly. The use of cellulose acetate, amino acids, and ionic liquids not only enhances the membrane properties but also aligns with sustainability goals, considering their renewable nature, reducing reliance on hazardous chemicals, and minimal environmental impact during fabrication. Furthermore, the cost-effectiveness, availability of materials and the simplicity of the fabrication process suggest that the membrane fabrication process can be scaled up for large-scale industrial applications.

Data availability

The authors confirm that the data supporting the findings of this study are available within the article. Should any raw data files be needed in another format, they are available from the corresponding author upon reasonable request.

Conflicts of interest

There are no conflicts to declare.

References

1 G. Arthanareeswaran, P. Thanikaivelan, N. Jaya, D. Mohan and M. Raajenthiren, Removal of chromium from aqueous solution using cellulose acetate and sulfonated poly(ether ether ketone) blend ultrafiltration membranes, *J. Hazard. Mater.*, 2007, **139**(1), 44–49.

2 R. Shrestha, S. Ban, S. Devkota, S. Sharma, R. Joshi, A. P. Tiwari, *et al.*, Technological trends in heavy metals removal from industrial wastewater: A review, *J. Environ. Chem. Eng.*, 2021, **9**(4), 105688.

3 A. Singhal, Heavy metals in drinking water and their impact on human health, *Asian J. Res. Soc. Sci. Humanit.*, 2021, **11**(11), 586–591.

4 M. Li, Q. Shi, N. Song, Y. Xiao, L. Wang, Z. Chen, *et al.*, Current trends in the detection and removal of heavy metal ions using functional materials, *Chem. Soc. Rev.*, 2023, **52**(17), 5827–5860.

5 Y. Tang, L. Zhang, X. Ge, Y. Zhang, Y. Liu and J. Wang, A mild one-step method to fabricate graphene oxide cross-linked with dopamine/polyethyleneimine (GO@DA/PEI) composite membranes with an ultrahigh flux for heavy metal ion removal, *Sep. Purif. Technol.*, 2024, **339**, 126618.

6 N. A. A. Qasem, R. H. Mohammed and D. U. Lawal, Removal of heavy metal ions from wastewater: a comprehensive and critical review, *npj Clean Water*, 2021, **4**(1), 36.

7 F. Fu and Q. Wang, Removal of heavy metal ions from wastewaters: A review, *J. Environ. Manage.*, 2011, **92**(3), 407–418.

8 N. Rossignol, L. Vandanjon, P. Jaouen and F. Quéméneur, Membrane technology for the continuous separation microalgae/culture medium: compared performances of cross-flow microfiltration and ultrafiltration, *Aquac. Eng.*, 1999, **20**, 191–208.

9 H. Salem, E. Eweida and A. Faraq, *Heavy Metals in Drinking Water and Their Environmental Impact on Human Health*, Cairo Univ., 2000, pp. 542–56.

10 M. D. Islam, F. J. Uddin, T. U. Rashid and M. Shahruzzaman, Cellulose acetate-based membrane for wastewater treatment—A state-of-the-art review, *Mater. Adv.*, 2023, **4**(18), 4054–4102.

11 D. Han and K. H. Row, Recent applications of ionic liquids in separation technology, *Molecules*, 2010, **15**(4), 2405–2426.

12 M. Fuerhacker, T. M. Haile, D. Kogelnig, A. Stojanovic and B. Keppler, Application of ionic liquids for the removal of heavy metals from wastewater and activated sludge, *Water Sci. Technol.*, 2012, **65**(10), 1765–1773.

13 D. B. Williams, M. E. Stoll, B. L. Scott, A. Costa and W. J. Oldham, Coordination chemistry of the bis(trifluoromethylsulfonyl)imide anion: molecular interactions in room temperature ionic liquids, *Chem. Commun.*, 2005, **613**(1), 1438–1440.

14 K. S. Aditya, Y. Lukka Thuyavan, G. Arthanareeswaran, T. Matsuura and A. F. Ismail, Impact of graphene oxide embedded polyethersulfone membranes for the effective treatment of distillery effluent, *Chem. Eng. J.*, 2016, **286**, 528–537.

15 G. Arthanareeswaran, K. Srinivasan, R. Mahendran, D. Mohan, M. Rajendran and V. Mohan, Studies on cellulose acetate and sulfonated poly(ether ether ketone) blend ultrafiltration membranes, *Eur. Polym. J.*, 2004, **40**(4), 751–762.

16 S. Hafeez, X. Fan and A. Hussain, A Kinetic Study of CO_2 Adsorption in Cellulose Acetate Membranes, *Int. J. Environ. Sci. Dev.*, 2015, **6**(10), 755–759.

17 P. Xing, G. P. Robertson, M. D. Guiver, S. D. Mikhailenko, K. Wang and S. Kaliaguine, Synthesis and characterization of sulfonated poly(ether ether ketone) for proton exchange membranes, *J. Membr. Sci.*, 2004, **229**(1–2), 95–106.

18 S. K. R, G. Arthanareeswaran, L. T. Y and A. F. Ismail, Journal of the Taiwan Institute of Chemical Engineers Enhancement of permeability and antibiofouling properties of polyethersulfone (PES) membrane through incorporation of quorum sensing inhibition (QSI) compound, *J. Taiwan Inst. Chem. Eng.*, 2017, **72**, 200–212.

19 G. Gnanasekaran, A. G and Y. S. Mok, A high-flux metal-organic framework membrane (PSF/MIL-100 (Fe)) for the removal of microplastics adsorbing dye contaminants from textile wastewater, *Sep. Purif. Technol.*, 2021, **277**(September), 119655.

20 F. Zhao, H. Chu, Z. Yu, S. Jiang, X. Zhao, X. Zhou, *et al.*, The filtration and fouling performance of membranes with different pore sizes in algae harvesting, *Sci. Total Environ.*, 2017, **587–588**, 87–93.

21 A. K. Shukla, J. Alam, M. A. Ansari, M. Alhoshan, M. Alam and A. Kaushik, Selective ion removal and antibacterial activity of silver-doped multi-walled carbon nanotube/polyphenylsulfone nanocomposite membranes, *Mater. Chem. Phys.*, 2019, **233**(April), 102–112.

22 W. Hu, Y. Ma, Z. Zhan, D. Hussain and C. Hu, Robotic Intracellular Electrochemical Sensing for Adherent Cells, *Cyborg Bionic Syst.*, 2022, **2022**, 9763420.

23 W. P. Zhu, J. Gao, S. P. Sun, S. Zhang and T. S. Chung, Poly(amidoamine) dendrimer (PAMAM) grafted on thin film composite (TFC) nanofiltration (NF) hollow fiber membranes for heavy metal removal, *J. Membr. Sci.*, 2015, **487**, 117–126.

24 M. Alhoshan, J. Alam, A. K. Shukla and A. A. Hamid, Polyphenylsulfone membrane blended with polyaniline for nanofiltration promising for removing heavy metals (Cd^{2+}/Pb^{2+}) from wastewater, *J. Mater. Res. Technol.*, 2023, **24**, 6034–6047.

25 Z. Wang, C. Fernández-Blanco, J. Chen, M. C. Veiga and C. Kennes, Effect of electron acceptors on product selectivity and carbon flux in carbon chain elongation with Megasphaera hexanoica, *Sci. Total Environ.*, 2024, **912**, 169509.

26 K. Tan, C. Li, H. Meng and Z. Wang, Improvement of hydrophobicity of ionic liquids by partial chlorination and fluorination of the cation, *Chin. J. Chem.*, 2009, **27**(1), 174–178.

27 Z. Xiong, J. Liu, Y. Yang, Q. Lai, X. Wu, J. Yang, *et al.*, Reinforcing hydration layer on membrane surface via nano-capturing and hydrothermal crosslinking for fouling reduction, *J. Membr. Sci.*, 2022, **644**(September 2021), 120076, DOI: **10.1016/j.memsci.2021.120076**.

28 H. Mohamed, S. Hudziak, V. Arumuganathan, Z. Meng and M. O. Coppens, Effects of charge and hydrophilicity on the anti-fouling properties of kidney-inspired, polyester membranes, *Mol. Syst. Des. Eng.*, 2020, **5**(7), 1219–1229.

29 K. M. Alotaibi, A. K. Shukla, E. Bajuayfir, A. A. Alotaibi, M. H. Mrad, F. A. Gomaa, *et al.*, Ultrasound-assisted synthesis of MSNs/PS nanocomposite membranes for effective removal of Cd^{2+} and Pb^{2+} ions from aqueous solutions, *Ultrason. Sonochem.*, 2023, **98**(June), 106497.

30 L. Chancelier, O. Boyron, T. Gutel and C. Santini, Thermal stability of imidazolium-based ionic liquids, *Fr.-Ukr. J. Chem.*, 2016, **4**(1), 51–64.

31 T. Hwang, Y. K. Oh, B. Kim and J. I. Han, Dramatic improvement of membrane performance for microalgae harvesting with a simple bubble-generator plate, *Bioresour. Technol.*, 2015, 343–347.

32 Z. Fallah, E. N. Zare, M. A. Khan, S. Iftekhar, M. Ghomi, E. Sharifi, et al., Ionic liquid-based antimicrobial materials for water treatment, air filtration, food packaging and anticorrosion coatings, Adv. Colloid Interface Sci., 2021, **294**, 102454.

33 X. Wang, K. Zhou, Z. Ma, X. Lu, L. Wang, Z. Wang, et al., Preparation and characterization of novel polyvinylidene fluoride/2-aminobenzothiazole modified ultrafiltration membrane for the removal of Cr(VI) in wastewater, Polymers, 2018, **10**(1), 19.

34 A. Abidi, N. Gherraf, S. Ladjel, M. Rabiller-Baudry and T. Bouchami, Effect of operating parameters on the selectivity of nanofiltration phosphates transfer through a Nanomax-50 membrane, Arabian J. Chem., 2016, **9**, S334–S341.

35 A. K. Shukla, J. Alam, M. Alhoshan, L. Arockiasamy Dass, F. A. A. Ali, M. R. Muthumareeswaran, et al., Removal of heavy metal ions using a carboxylated graphene oxide-incorporated polyphenylsulfone nanofiltration membrane, Environ. Sci.:Water Res. Technol., 2018, **4**(3), 438–448.

36 X. Wei, X. Kong, S. Wang, H. Xiang, J. Wang and J. Chen, Removal of Heavy Metals from Electroplating Wastewater by Thin- Film Composite Nano filtration Hollow-Fiber Membranes, Ind. Eng. Chem. Res., 2013, **52**(49), 17583–17590.

37 P. Aydogan Gokturk, R. Sujanani, J. Qian, Y. Wang, L. E. Katz, B. D. Freeman, et al., The Donnan potential revealed, Nat. Commun., 2022, **13**(1), 5880.

38 Y. Wang, Y. Xu, W. Zhai, Z. Zhang, Y. Liu, S. Cheng, et al., In-situ growth of robust superlubricated nano-skin on electrospun nanofibers for post-operative adhesion prevention, Nat. Commun., 2022, **13**(1), 5056.

39 G. Gnanasekaran, S. Balaguru, G. Arthanareeswaran and D. B. Das, Removal of hazardous material from wastewater by using metal organic framework (MOF) embedded polymeric membranes, Sep. Sci. Technol., 2019, **54**(3), 434–446.

40 J. Torkashvand, A. Saeedi-Jurkuyeh, R. Rezaei Kalantary, M. Gholami, A. Esrafili, M. Yousefi, et al., Preparation of a cellulose acetate membrane using cigarette butt recycling and investigation of its efficiency in removing heavy metals from aqueous solution, Sci. Rep., 2022, **12**(1), 1–11.

41 S. Acarer-Arat, İ. Pir, M. Tüfekci, S. Güneş-Durak, A. Akman and N. Tüfekci, Heavy Metal Rejection Performance and Mechanical Performance of Cellulose-Nanofibril-Reinforced Cellulose Acetate Membranes, ACS Omega, 2024, 42061–42090.